Proceedings of the 7th International Symposium on Cavitation
CAV2009-Paper No. 67
August 17-22, 2009, Ann Arbor, Michigan, USA

Numerical Prediction of Cavitation Erosion in Cavitating Flow

Naoya Ochiai
Graduate School of Tohoku Univ.
Sendai, JAPAN

Yuka Iga
Institute of Fluid Science, Tohoku Univ.
Sendai, JAPAN

Motohiko Nohmi
EBARA Corporation
Tokyo, JAPAN

Toshiaki Ikohagi
Institute of Fluid Science, Tohoku Univ.
Sendai, JAPAN

ABSTRACT

In this study bubble behavior in cavitating flow is analyzed and prediction of cavitation erosion in 2D cavitating flow around ClarkY 11.7 % hydrofoil at several cavitation is performed by impact pressure induced by bubble collapse. Our numerical method predicts that the impact energy is small if variation of cavitating flow is small and that the position of peak impact energy moves downstream with the decrease in cavitation number until the maximum sheet cavity length becomes larger than chord length. When the maximum sheet cavity length becomes larger than chord length, there are not obvious peak values and relatively weak erosion occurs. And it is found that high impact pressures are mainly induced by bubbles in a cloud and in the vicinity of sheet cavity termination during a cloud collapse. Therefore large impact energy occurs when the cloud cavity collapses near the hydrofoil, the sheet cavity termination is on the hydrofoil and the number of bubble is large in these cavities.

INTRODUCTION

Cavitation erosion is a severe problem which causes material fracture of fluid machineries because of violent collapse of a cavitation bubble or bubble cluster when they arrive at a region where ambient pressure recovers. Collapse of a cavitaion bubble is high speed and local phenomenon, and the repetition causes erosion on material surface when fluid machinery operates for a long time on cavitation. Development of prediction of intensity of cavitating flow or amount of cavitation erosion is concerned from industrial point of view that it demands to evaluate cavitation erosion without long time experiment of cavitation erosion. There are many works about prediction of cavitation erosion. For example, Szkodo [1] proposed a mathematical modeling of volume loss curve to time which assumed that probability of volume loss in elementary volume is described by Weibull's function. Franc and Riondet [2] proposed a erosion model in which it is assumed that no mass loss appears and workhardening process occurs when a stress acting on a material is weaker than the ultimate tensile strength of the material, and mass loss starts when cumulative energy of a material reaches the energy corresponding to the ultimate tensile strength. Dular et al. [3] showed a relationship between cavitation erosion and cavitation aspect, and evaluated the erosion of a hydrofoil surface assuming that the strength of shock wave occurred by a cloud cavitation collapse is proportional to the velocity of change of cloud volume. Fukaya et al. [4] proposed numerical prediction method of cavitation erosion to evaluate cavitation intensity using bubble internal pressure and number density of bubble. However there has not been the practical numerical method yet because cavitation erosion is related to a complex phenomenon owing to microscopic bubble or bubble cluster collapse.

Two mechanisms of occurrence of cavitation erosion have been proposed. One is that shock wave radiated from a rebounding bubble causes cavitation erosion (e.g. Hickling and Plesset [5], and Fujikawa and Akamatsu [6]), and another is that microjet generated from a collapsing bubble near the material surface causes cavitation erosion (e.g. Naude and Ellis [7], and Plesset and Chapman [8]). It is important that high speed and local motion of bubble in cavitating flow is considered for predicting cavitation erosion numerically regardless of which standpoint is correct. And intensity of cavitating flow changes with flow conditions, e.g. flow velocity and cavitaion number (e.g. He and Hammitt [9], and Van der Meulen and Nakashima [10]). Therefore it is necessary to understand characteristics of cavitating flow and cavitation bubbles in the flow field to predict cavitation erosion.

In this study bubble behavior in cavitating flow is analyzed and prediction of cavitation erosion is performed numerically. Numerical simulation of macroscopic cavitating flow and microscopic bubble in the flow are performed by locally homogeneous model and bubble dynamics respectively. These calculations are coupled by one way from cavitating flow to bubble motion. Prediction of cavitation erosion is performed by the impact pressure induced by bubble collapse and rebound assuming that the impact pressure causes cavitation erosion. 2D cavitating flows around ClarkY 11.7 % hydrofoil at several cavitation number are picked up to examine our prediction method. Cavitation erosion on attached cavitating flow, transient cavitating flow, supercavitating flow is predicted and the relationships between flow field and cavitation erosion are analysed.

NUMERICAL METHOD

<Macroscopic Numerical Method of Cavitating Flow>

Gas-liquid two phase Navier-Stokes equation is solved by using locally homogeneous model of gas-liquid two phase medium (Okuda and Ikohagi [11], and Iga et al. [12]) to simulate macroscopic cavitating flow efficiently. This model treats two phase medium as a pseudo single-phase medium which has locally homogeneous void fraction. It is assumed that liquid phase follows Tamman type equation of state and that gas phase follows equation of state of ideal gas. The equation of state of two phase medium is expressed by using mass fraction of gas Y as follows:

$$\rho = \frac{p(p+p_c)}{K_l(1-Y)p(T+T_0)+R_gY(p+p_c)T}, \tag{1}$$

where p_c, K_l, T_0 and R_g are liquid pressure constant, liquid constant, liquid temperature constant and gas constant.

In this study, cavitating flow is treated as air-water-vapor two-component two phase medium. Governing equations are continuity equation, momentum equation, total energy equation of two phase compressible medium, and continuity equations of mixture gas phase, and expressed as follows:

$$\frac{\partial \boldsymbol{Q}}{\partial t} + \frac{\partial (\boldsymbol{E}_j - \boldsymbol{E}_{vj})}{\partial x_j} = \boldsymbol{S}, \tag{2}$$

$$\boldsymbol{Q} = \begin{bmatrix} \rho \\ \rho u_i \\ e \\ \rho Y \\ \rho Y D_a \end{bmatrix}, \ \boldsymbol{E}_j = \begin{bmatrix} \rho u_j \\ \rho u_i u_j + \delta_{ij} p \\ \rho u_j H \\ \rho u_j Y \\ \rho u_j Y D_a \end{bmatrix}, \ \boldsymbol{E}_{vj} = \begin{bmatrix} 0 \\ \tau_{ij} \\ q_j + \tau_{jk} u_k \\ 0 \\ 0 \end{bmatrix},$$

$$\tau_{ij} = (\mu + \mu_t)\left(\frac{\partial u_i}{\partial x_j} + \frac{\partial u_j}{\partial x_i} - \frac{2}{3}\delta_{ij}\frac{\partial u_k}{\partial x_k}\right), \tag{3}$$

$$q_j = -(\kappa + \kappa_t)\frac{\partial T}{\partial x_j}, \tag{4}$$

$$\mu = (1-\alpha)(1+2.5\alpha)\mu_l + \alpha\mu_g, \tag{5}$$

$$\kappa = (1-\alpha)\kappa_l + \alpha\kappa_g, \tag{6}$$

where $H = (e+p)/\rho$, τ_{ij}, q_j, μ and κ are total entalpy per unit mass, stress tensor, heat flux, viscosity and heat conductivity. Total energy per unit volume e is expressed as follows assuming that the entalpy per unit mass h is linear function with respect to T, $h = C_{pm}T + h_{0m}$, where C_{pm} and h_{0m} are specific heat at constant pressure and entalpy constant of two phase medium.

$$e = \rho\left(h - \frac{p}{\rho} + \frac{1}{2}u_i^2\right). \tag{7}$$

And $\boldsymbol{S} = [0, 0, 0, \dot{m}, 0]^{-1}$, where $\dot{m}$ is phase change term. Evaporation or condensation rate per unit surface area at interface $\dot{m}_b$ is expressed by Hertz-Knudsen-Langumiur's equation.

$$\dot{m}_b = \frac{C_{e/c}}{\sqrt{2\pi R_{gv}}}\left(\frac{p_v^*}{\sqrt{T}} - \frac{p_v}{\sqrt{T_b}}\right), \tag{8}$$

where $C_{e/c}$, T_b, p_v^*, p_v and R_{gv} are evaporation or condensation coefficient at bubble wall, temperature in a bubble, saturated vapor pressure, partial pressure of vapor and gas constant of vapor. Evaporation or condensation rate per unit volume in two phase medium $\dot{m}$ is modelled as follows assuming $T_b = T$ and using representative bubble radius R_{rep} and bubble number density n.

$$\dot{m} = n4\pi R_{\mathrm{rep}}^2 C_{e/c}\frac{p_v^* - p_v}{\sqrt{2\pi R_{gv}T}}. \tag{9}$$

Further it is approximated that $n = \alpha(1-\alpha)/(4\pi R_{\mathrm{rep}}^3/3)$, where $\alpha \approx 0$, $\alpha \approx n4\pi R_{\mathrm{rep}}^3/3$ and $\alpha \approx 1$, $1-\alpha \approx n4\pi R_{\mathrm{rep}}^3/3$. Finally $\dot{m}$ is expressed as follows:

$$\dot{m} = \alpha(1-\alpha)\frac{4\pi R_{\mathrm{rep}}^2}{\frac{4}{3}\pi R_{\mathrm{rep}}^3}C_{e/c}\frac{p_v^* - p_v}{\sqrt{2\pi R_{gv}T}} = \alpha(1-\alpha)AC_{e/c}\frac{p_v^* - p_v}{\sqrt{2\pi R_{gv}T}}, \tag{10}$$

where A is interfacial area concentration in the gas-liquid mixture and

$$A = \frac{3}{R_{\mathrm{rep}}} = 3\left(\frac{4}{3}\pi n\right)^{\frac{1}{3}}\alpha^{-\frac{1}{3}}(1-\alpha)^{-\frac{1}{3}} = C_a\alpha^{-\frac{1}{3}}(1-\alpha)^{-\frac{1}{3}}. \tag{11}$$

In this study, model constants C_eC_a and C_cC_a are set to 1000 and 1 [m^{-1}].

C_{pm} and h_{0m} are expressed by linearly combining C_{pl} and C_{pg}, and h_{0l} and h_{0g} with Y. C_{pg}, h_{0g} and R_g are respectively expressed by linearly combining C_{pa} and C_{pv}, h_{0a} and h_{0v}, and R_{ga} and R_{gv} with density ratio D_a of air in gas phase.

The discretization of finite volume method, ADI method for time integration, AUSM type upwind scheme (Shima and Jounouchi[13]) with 3rd-order MUSCL-TVD (Anderson et al. [14]) to evaluate numerical flux, Baldwin-Lomax model with Degani-Sciff modification (Degani and Schiff [15]) as turbulent model are used.

When the change of mass fraction of gas ΔY is large at the cell interface, higher order numerical flux may yields non-physical oscillation. Therefore 1st-order upwind scheme is used if $2|\Delta Y_{i-\frac{1}{2}}| > |\Delta Y_{i+\frac{1}{2}}|$ or $2|\Delta Y_{i+\frac{1}{2}}| > |\Delta Y_{i-\frac{1}{2}}|$ or $2|\Delta Y_{i+\frac{1}{2}}| > |\Delta Y_{i+\frac{3}{2}}|$ or $2|\Delta Y_{i+\frac{3}{2}}| > |\Delta Y_{i+\frac{1}{2}}|$ at the cell $i+\frac{1}{2}$.

<Microscopic Numerical Method of Cavity Bubble>

It is assumed that bubble remains spherical shape and follows equation of bubble motion which contains forces only by pressure gradient ∇p, drag force $\boldsymbol{F}_D$ and virtual mass force $\boldsymbol{F}_{VM}$ as follows:

$$\rho_b V_b \frac{d\boldsymbol{u}_b}{dt} = -V_b \nabla p - \boldsymbol{F}_D + \boldsymbol{F}_{VM}, \tag{12}$$

where ρ_b, V_b and $\boldsymbol{u}_b$ are density, volume and velocity vector of bubble.

In order to evaluate bubble radius, the equation of bubble oscillation considering liquid compressibility up to the first order in bubble wall Mach number and phase change at bubble wall is used (Keller and Kolodner [16] and Yasui [17]).

$$\begin{aligned} &R\ddot{R}\left(1 - \frac{\dot{R}}{C} + \frac{\dot{m}_b}{\rho C}\right) + \frac{3}{2}\dot{R}^2\left(1 - \frac{1}{3}\frac{\dot{R}}{C} + \frac{2}{3}\frac{\dot{m}_b}{\rho C}\right) \\ &-\frac{1}{2}\frac{\dot{m}_b}{\rho}\left(2\dot{R} + \frac{\dot{m}_b}{\rho} + \frac{\dot{R}\dot{m}}{\rho C}\right) - \frac{R\ddot{m}_b}{\rho}\left(1 - \frac{\dot{R}}{C} + \frac{\dot{m}}{\rho C}\right) \\ &= \frac{1}{\rho}\left(1 + \frac{\dot{R}}{C} + \frac{R}{C}\frac{d}{dt}\right)\left(p_a + p_v - p - \frac{4\mu\dot{R}}{R} - \frac{2\sigma_{st}}{R}\right) \end{aligned} \tag{13}$$

where p_a, p_v, ρ, C, μ and σ_{st} are partial pressure of air and vapor in a bubble, density, speed of sound, viscosity and surface tension coefficient of ambient fluid and dot denotes derivative

respect to time. In this study, it is assumed that vapor and air (noncondensable gas) are involved in a bubble microscopically. In order to calculate partial pressures of vapor and air, continuity equations of vapor and air in a bubble are used.

$$\frac{d}{dt}\left(\frac{4}{3}\pi R^3\rho_v\right) = 4\pi R^2\dot{m}_b, \tag{14}$$

$$\frac{d}{dt}\left(\frac{4}{3}\pi R^3\rho_a\right) = 0. \tag{15}$$

And in order to evaluate temperature in a bubble, energy equation of mixture gas in a bubble is solved([18]).

$$\frac{d}{dt}\left(\frac{4}{3}\pi R^3\rho_{mg}U_{mg}\right) = -p_{mg}\frac{d}{dt}\left(\frac{4}{3}\pi R^3\right) - 4\pi R^2\delta U. \tag{16}$$

Specific internal energy of mixture gas in a bubble $U_{mg} = (\rho_v C_{vv} + \rho_a C_{va})T_b/\rho_{mg}$ where C_{vv} and C_{va} are specific heat of vapor and air at constant volume, and δU is energy flux at bubble wall. Initial p_v is assumed saturated vapor pressure and p_a is then calculated from the condition which force equilibrium condition at bubble wall is kept (initial bubble wall velocity $\dot{R} = 0$). Equations of bubble motion and bubble oscillation are solved using 4th-order Runge-Kutta method.

Physical values of liquid phase from macroscopic calculation are used for reference physical values of bubble calculation. Macroscopic analysis of cavitating flow and microscopic analysis of cavitation bubble are coupled by one-way coupling algorithm from macroscopic analysis to microscopic analysis. Because time scales of macroscopic flow and bubble collapse are different greatly, time step for bubble oscillation is determined as 0.01 dt where dt is time step for macroscopic flow field.

<Evaluation Method of Impact Pressure Owing to Pressure Wave Induced by Bubble Collapse>

In this study, prediction of cavitation erosion is performed by the impact pressure owing to pressure wave induced by bubble collapse.

It is assumed that pressure field in the vicinity of a bubble which collapses and induces the pressure wave is that of potential flow induced by spherical motion of the bubble. Next equation is obtained using velocity potential ϕ of the flow field.

$$\frac{\partial^2\phi}{\partial t\partial r} + \frac{\partial\phi}{\partial r}\frac{\partial^2\phi}{\partial r^2} = -\frac{\partial p}{\partial r}. \tag{17}$$

ϕ is the solution of wave equation propagating to ambient liquid and expressed considering that liquid compressibility up to the first order of $1/C$ as follows:

$$\phi = \frac{1}{r}f\left(t - \frac{r-R}{C}\right) = \frac{1}{r}\left(-R^2\dot{R} + \frac{1}{C}\left(R^3\ddot{R} + 2R^2\dot{R}^2\right)\right). \tag{18}$$

Substituting ϕ expressed by Eq. (18) to Eq. (17) and integrating this equation from $r = r$ to $r = \infty$, pressure p_r at position r from the center of bubble is expressed as follows.

$$p_r = p - \rho\left(\frac{f'}{r} + \frac{1}{2}\left(\frac{f^2}{r^4} + \frac{2}{C}\frac{ff'}{r^3} + \frac{1}{C^2}\frac{f'^2}{r^2}\right)\right), \tag{19}$$

where a prime indicates differential with respect to $t-(r-R)/C$.

Impact pressure acting on material surface P_w is calculated by Eq. (19) substituting a distance between a position of bubble collapse and material surface to r in Eq. (19).

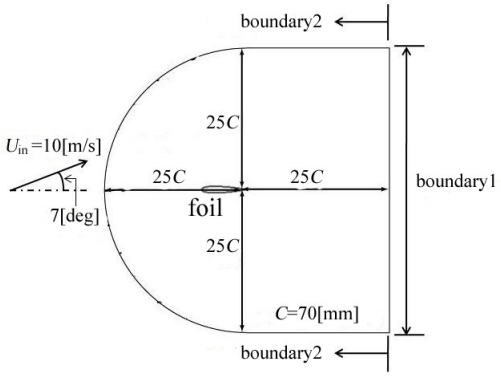

Figure 1: Calculation area

CALCULATION CONDITION

Cavitating flow around ClarkY11.7% (chord length 70[mm]) 2D hydrofoil is analyzed. Figure 1 shows the calculation area. C-type grid system with 257×85 (streamwise × perpendicular direction) grid points is used. Mainflow velocity, temperature and void fraction are 10[m/s], 293.15[K] and 0.1% respectively and angle of attack is 7[deg]. The wall boundary condition is non-slip condition and $\partial\boldsymbol{Q}/\partial n = 0$ at boundary 1 where n is the perpendicular direction to the boundary, and density, velocity, static pressure, temperature and mass fraction of gas are constant at boundary 2.

Cavitation number σ is defined as follows:

$$\sigma = \frac{p_{in} - p_v^*(T_{in})}{\frac{1}{2}\rho_{in}U_{in}^2}. \tag{20}$$

For bubble calculations, initial bubble radius is $R_0 = 0.1$[mm], initial positions (x, y) are five points (-3, 1.00), (-3, 2.75), (-3, 4.50), (-3, 6.25), (-3, 8.00)[mm](x is hydrofoil chord direction, y is the perpendicular direction to x and the origin of this coordinate is hydrofoil leading edge), and five bubbles are released at five initial positions every 0.2[ms].

RESULTS AND DISCUSSION

<Numerical Analysis of Cavitating Flow at Several Cavitation Number>

Calculations at several cavitation number for above mentiones constant main flow velocity, temperature and void fraction are performed. Main flow pressure changes along with σ. Figures 2 and 3 show calculated and experimental (Numachi. et al [19]) time average lift coefficients and standard deviations of lift coefficients, and maximum and average sheet cavity length (l_{cav}/c, where l_{cav} is a length of sheet cavity from hydrofoil leading edge) and standard deviation of l_{cav}/c at several σ, respectively. First comparing calculated and experimental average lift coefficients, it seems that in this calculations simulated average C_L agree well with experimental values although average C_L are underestimated for $1.1 \leqq \sigma \leqq 1.4$. At $\sigma = 2.0$ the sheet cavity length is zero as shown in Fig. 3 and the flow field is noncavitating flow. And the variation of C_L is small as shown in Fig. 2. At $1.3 \leqq \sigma \leqq 1.6$ sheet cavitation occurs from hydrofoil leading edge and the variation of C_L is small and it is found that attached cavitating flow occurs stably. At $\sigma = 1.2$ maximum sheet cavity length is larger than 60 % c and the variation of C_L becomes large and it is found that transient cavitating flow occurs with generations and collapses of

cloud cavity. At this σ the difference between calculated and experimental average C_L is largest. At $0.5 \leqq \sigma \leqq 1.1$ standard deviations of C_L is large too and transient cavitating flow prevails at these σ. The standard deviation of C_L is the largest at $\sigma = 0.8$ At $0.5 \leqq \sigma \leqq 0.8$, l_{cav} is larger than chord length and as σ becomes small, the standard deviation of C_L becomes small. At σ lower than 0.4 the standard deviation of C_L is small as shown in Fig. 2 and l_{cav} is much larger than chord length and it is found that pseudo supercavitating flow occurs at these σ.

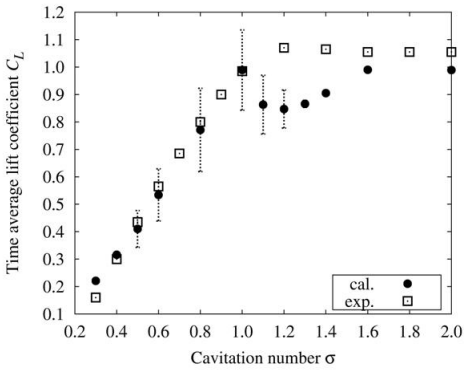

Figure 2: Time average lift coefficient and standard deviation of lift coefficient at several cavitation number

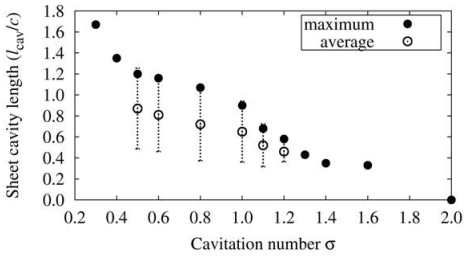

Figure 3: Maximum and average sheet cavity length and standard deviation of sheet cavity length for transient cavitating flow at several cavitation number

Next the analyses of cavitating flow are performed in detail at $0.6 \leqq \sigma \leqq 1.2$ where the standard deviations of C_L are large in transient cavitating flow. Figure 4 shows time histories of C_L at $\sigma = 1.2$, 1.1, 1.0 and 0.6. At $\sigma = 1.2$ collapses of cloud cavity occur irregularly at about 9, 20, 44, 82 and 89[ms] and there are small cloud cavities due to partial separation of sheet cavities and large cloud cavities which roll up after the sheet cavities break off (Fig. 4 (i)). The small cloud cavities collapse at 9, 20 and 89[ms] and large cloud cavities collapse at 44 and 82[ms]. At $\sigma = 1.1$ collapses of small and large cloud cavity occur rather periodically at about 13, 24, 39, 50, 65, 77 and 92[ms] (Fig. 4 (ii)), where small and large cloud cavities collapse in $0.7 < x/c < 0.8$ and $0.9 < x/c < 1.0$ at 24, 50, 77[ms] and 13, 39, 65, 92[ms], respectively. At $\sigma = 1.0$ collapses of large cloud cavity in the same size occur periodically at 4, 23, 42, 61 and 80[ms] (Fig. 4 (iii)). At $0.5 \leqq \sigma \leqq 0.8$ periodic cavitating flow with generation and collapse of large cloud cavity occur as well as at $\sigma = 0.6$ (Fig. 4 (iv)). At $\sigma \leqq 1.0$ cloud cavities collapse at the downstream of the hydrofoil trailing edge (this is because maximum sheet cavity length is larger than chord length (Fig. 3)). Rapid variations of C_L are found in Fig. 4 at the times of collapse of cloud cavity because the collapses can cause high pressure. At $\sigma = 1.2$, 1.1 local minimum values of C_L correspond to the times of collapse of cloud cavity because the cloud cavities collapse on the hydrofoil and high pressures act directly on the suction side of the hydrofoil. On the other hand, at $0.5 \leqq \sigma \leqq 1.0$ local maximum values of C_L correpond to the times because the cloud cavities collapse at the downstream of hydrofoil trailing edge and high pressures propagate not to the suction side but to the pressure side of the hydrofoil. At these σ next sheet cavities have already grown up when the cloud cavities collapse and therefore it is thought that high pressures can hardly propagate to the suction side (attenuation of pressure wave is larger in high void region than in liquid region). Also, it is thought that there are non-periodic collapse of small and large cloud cavities at $\sigma = 1.2$ because pressure waves owing to cloud collapses influence on the development of sheet cavities in the upstream suction side.

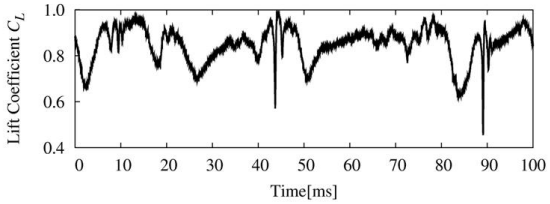

(i) $\sigma = 1.2$

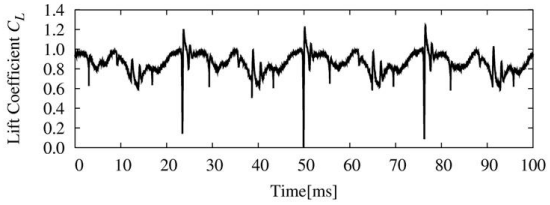

(ii) $\sigma = 1.1$

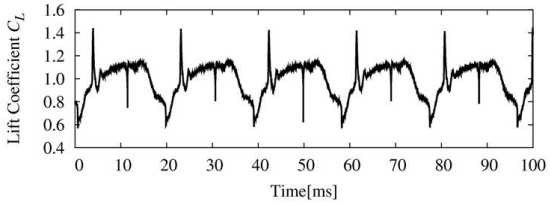

(iii) $\sigma = 1.0$

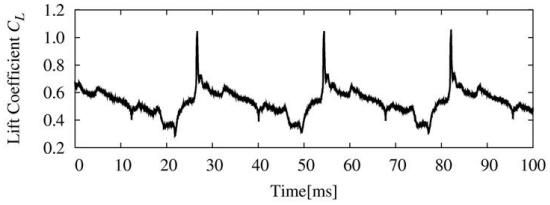

(iv) $\sigma = 0.6$

Figure 4: Time histories of lift coefficient

<**Numerical Analysis of Bubble Behavior at Several Cavitation Number**>

In this section, at several σ and the behavior of representative bubble in cavitating flow is analysed at each σ. Figure 5 shows ambient pressure and radius of representative bubble at σ =2.0 (noncavitating flow), 1.4 (attached cavitating flow) and

0.3 (pseudo supercavitating flow). Abscissa axis of Fig. 5 is x cordinate of bubble position. At $\sigma = 2.0$ the bubble grows up to about two times larger than initial bubble radius R_0 owing to decrease in ambient pressure, but the bubble does not show violent collapse because ambient pressure recovers gradually. Therefore the bubbles does not induce high pressure wave and it is confirmed that the intensity of cavitation erosion in non-cavitating flow is extremely weak. At $\sigma = 1.4$ the bubble grows up to about four times R_0 in low pressure region of cavitation and shows violent collapse at $0.3 \leqq x/c \leqq 0.4$. Since from Fig. 3 the sheet cavity termination is at $0.3 \leqq x/c \leqq 0.4$, the bubble is exposed to rapid pressure increase. It is thought that the cavitation erosion may occur in the vicinity of sheet cavity termination because the bubble collapses there. But the impact pressure acting on the hydrofoil is 0.3[MPa] and is not necessarily very large. At $\sigma = 0.3$ the sheet cavity extends to the hydrofoil trailing edge and the bubble collapses at the downstream of the hydrofoil. The impact pressure is 0.02[MPa] which is very small because the position of bubble collapse is far from the hydrofoil ($x/c = 1.6$). As described above, the cavitation intensities of quasi steady flow (noncavitating flow, attached cavitating flow and supercavitating flow) are relatively weak.

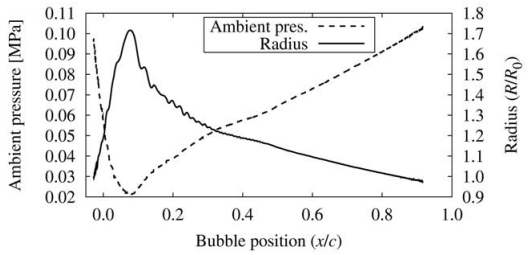

(i) $\sigma = 2.0$

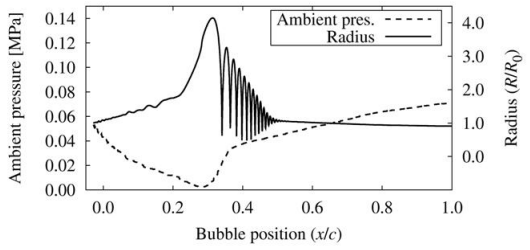

(ii) $\sigma = 1.4$

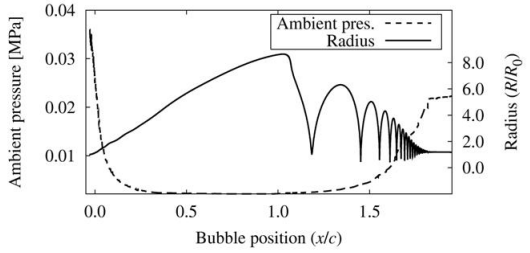

(iii) $\sigma = 0.3$

Figure 5: Ambient pressure and radius of representative bubble in quasi steady cavitating flow

Next, analysis of bubble behavior in $\sigma = 1.0$ is performed. At this σ transient cavitating flow occur with generations and collapses of cloud cavity and it is expected that the intensity of cavitation erosion is more strong than that of quasi steady cavitating flow. Figures 6 and 7 shows the trajectory of representative bubble and isoline of void fraction 0.1, and ambient pressure and radius of the representative bubble. This bubble exists near the interface of cloud cavity during the cloud cavity collapses. And this bubble is exposed to pressure increase at three times and shows rapid fluctuation at each times (Fig. 7). At about 58[ms] high impact pressure (about 70[MPa]) is induced.

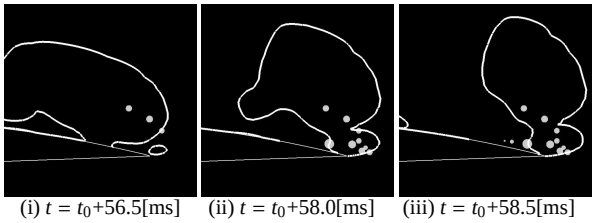

(i) $t = t_0$+56.5[ms] (ii) $t = t_0$+58.0[ms] (iii) $t = t_0$+58.5[ms]

Figure 6: Trajectory of representative bubble and isoline of void fraction 0.1 ($\sigma = 1.0$)

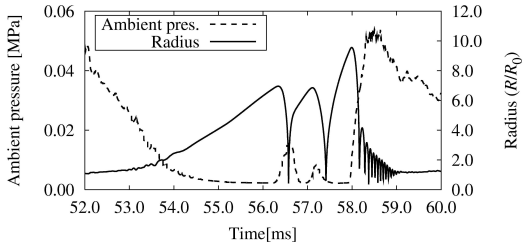

Figure 7: Ambient pressure and radius of representative bubble at $\sigma = 1.0$

<Prediction of Cavitation Erosion at Several Cavitation Number>

In this section, calculations of bubbles in cavitating flow at several σ and prediction of cavitation erosion are performed. Calculation times are 100[ms] for each σ. This time is longer than the time of 3-cycle of unsteady cavitating flow at $\sigma = 0.6$ (Fig. 4 (iv)). Soyama et al. [20] calculated individual impact energy E_i as follows:

$$E_i = I_i \tau_i A_i = \frac{P_i^2}{2\rho c} \tau_i A_i, \tag{21}$$

where I_i, τ_i, A_i and P_i are acoustic energy, impact duration, affective area and impact pressure. Following relation is obtained if ρ, c and τ_i are assumed constants.

$$E_i \propto P_i^2 A_i. \tag{22}$$

In this study $P_i^2 A_i$ is evaluated as follows using impact pressure P_w in infinitesimal area on the hydrofoil surface.

$$P_i^2 A_i = \int P_\mathrm{w}^2 dA, \tag{23}$$

where dA is the infinitesimal surface area with unit hydrofoil span for 2D calculation. Total energy of cavitation impacts E is described as follows:

$$E = \sum E_i \propto \sum \int P_\mathrm{w}^2 dA, \tag{24}$$

Figure 8 shows the relation between E and σ. It is found that E are almost zero at $\sigma \geqq 1.4$ or $\sigma \leqq 0.4$ since the variations of C_L at $\sigma \geqq 1.3$ or $\sigma \leqq 0.4$ are small as shown in Fig.

2, and there is a good correlation between cavitation erosion and variation of flow field. At $\sigma = 1.2$ the variation of C_L becomes large and E becomes large too. The maximum value of E occurs at $\sigma = 1.0$ in this study and E decreases gradually when σ decreases from 1.0. This is because cloud cavities collapse at downstream of the hydrofoil traliling edge at $\sigma \leqq 1.0$ as discussed in previous section and the frequencies of sheet cavity break off and cloud collapse decrease with the decrease in σ from 1.0 as shown in Fig. 4. Figure 9 shows the distributions of $\sum P_w^2$ at several σ. At $1.0 \leqq \sigma \leqq 1.2$ the position of maximum erosion moves to downstream with the decrease in σ. This is because sheet cavity termination and position of cloud cavity collapse move to downstream too. This movement corresponds well to experimental results that spatial maximum cavitation pressure pulse (Ito et al. [21]) and maximum damage (Dular et al. [3]) move away from the leading edge along with decrease in σ. These positions of maximum erosion are near the sheet cavity termination. At $\sigma = 0.8$ and 0.6 where the sheet cavity length are larger than chord length (Fig. 3), there are not the obvious peaks of cavitation erosion and weak erosion occur at wide region. Although E is almost equal at $\sigma = 1.2$, 1.1 and 0.8 (Fig. 8), the spatial distribution is different greatly (Fig. 9). The difference of the spatial distribution is closely related to the variation of sheet cavity length according to Magaino et al. [22]. When variation of l_{cav} is small ($\sigma = 1.2$) the spatial distribution has the obvious peak (Figs. 3 and 9) and the spatial distribution becomes broad with the increase in the variation. In this study maximum impact energy larger than twice that at $\sigma = 0.8$ occur locally at $\sigma = 1.2$.

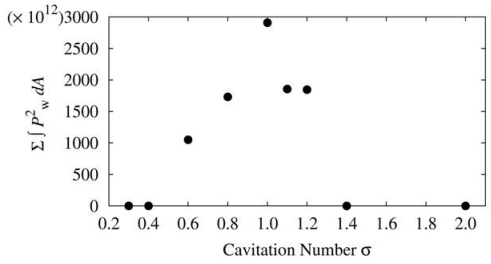

Figure 8: Relation between the total impact energy and cavitation number

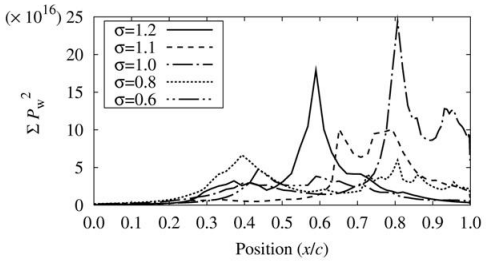

Figure 9: Distributions of impact energy at several cavitation number

Next the relationships between generation of impact pressures and flow field are analyzed at several σ. First, analysis at $\sigma = 1.0$ where maximum impact energy occur, is shown. Figures 10 and 11 show variation of C_L and $\Sigma \int P_w^2 dA$ every 1[ms] in one cycle of unsteady cavitating flow, and the time evolution of pressure distribution, isoline of void fraction 0.1, bubble positions and sizes at $\sigma = 1.0$, respectively. And Fig. 12 shows the distribution of impact energy at several times. One cycle of Fig. 10 is from the time of break off of sheet cavity to next break off and local minimum values of C_L indicate the times. Figure 11 (i) shows the time of first break off in the vicinity of the hydrofoil leading edge and the sheet cavity begins to flow downstream. It is found from Fig. 10 that E in this time is very small. E becomes large at about 53.0[ms] (Fig. 10). Figure 11 (ii) shows the aspect of flow field and bubbles at this time. It is thought that the interface of macroscopic cavity moves and the bubbles near the interface are exposed to high pressure gradient and collapse violently. Figure 11 (iii) shows the beginning of cloud cavity collapse and it is found that E at this time is large (at 58-59[ms] in Fig. 10). E in the vicinity of the hydrofoil trailing edge is large according to the distribution of impact energy at the time in Fig. 12. The area is near the position of the cloud cavity collapse and it is found that the bubbles in the cloud collapse violently and radiate high pressure wave. Figure 11 (iv) shows the time when very high pressure owing to macroscopic cloud cavity collapse occurs and E is the largest as shown in Fig. 10. The position of maximum impact energy is not at the hydrofoil trailing edge near the cloud cavity collapse but in the vicinity of the sheet cavity termination according to the distribution of impact energy at this time in Fig. 12. This means that the high pressure owing to macroscopic cloud collapse induces violent collapse of the bubbles in the vicinity of the sheet cavity termination. Comparing Fig. 12 to Fig. 9 it is found that impact energy

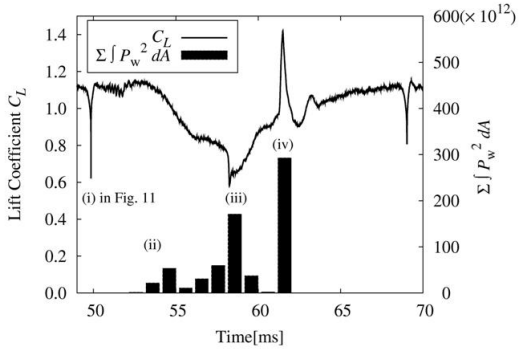

Figure 10: Variation of lift coefficient and $\Sigma \int P_w^2 dA$ every 1[ms] in one cycle of unsteady cavitating flow ($\sigma = 1.0$)

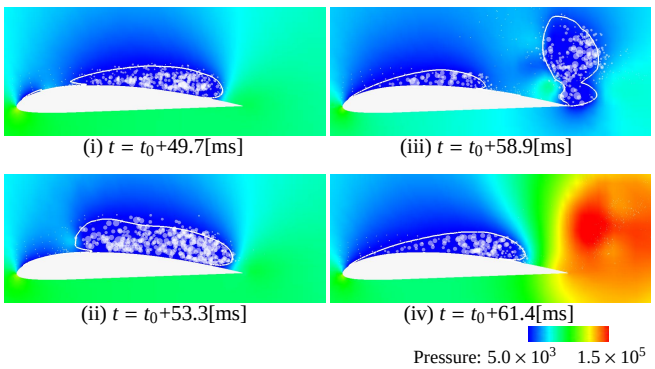

Figure 11: Time evolution of pressure distribution, isoline of void fraction 0.1, bubble positions and sizes ($\sigma = 1.0$)

owing to the bubbles in the vicinity of the sheet cavity termination corresponds to the peak impact energy at $x/c = 0.8$ and impact energy owing to the bubbles in the cloud corresponds to the second peak impact energy at $x/c = 0.95$.

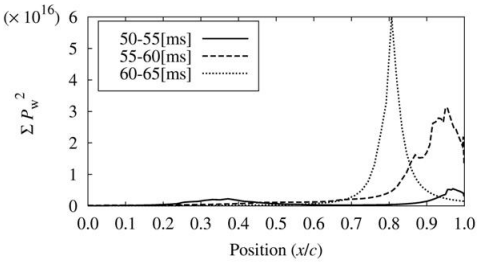

Figure 12: Distributions of impact energy at several times ($\sigma = 1.0$)

Second, analysis at $\sigma = 0.6$ where cavitation erosion is weak and the peak of impact energy is small, is shown. Figures 13 and 14 show variation of C_L and $\Sigma \int P_w^2 dA$ every 1[ms] in one cycle of unsteady cavitating flow, and the time evolution of pressure distribution, isoline of void fraction 0.1, bubble positions and sizes at $\sigma = 0.6$, respectively. E becomes large at 44-45[ms]. Macroscopic cavity moves downstream at the time and the bubbles near the interface collapse violently as well as at the time of Fig. 11 (ii) at $\sigma = 1.0$ (Fig. 14 (i)). However, there are not impact energies owing to the bubbles in the cloud and in the vicinity of the sheet cavity termination at the end of the cloud collapse (at 50-55[ms] in Fig. 13). The cloud cavity collapses far from the hydrofoil as shown in Fig. 14 (ii). The pressure waves radiated by the bubbles in the cloud at the cloud collapse are attenuated largely and do not contribute to impact pressures. Since the sheet cavity length is about chord length, the surface pressure increase in the vicinity of the sheet cavity termination induced by the cloud collapse are smaller than these at $\sigma = 1.0$. Therefore, the bubbles in the vicinity of the sheet cavity termination don't collapse violently too and E is small at the time. And it is thought that there is no obvious peak in the distribution of impact energy at $\sigma = 0.6$ as shown in Fig. 9 because there are not these occurrences of impact energy, which cause the first and second peak at $\sigma = 1.0$ (Fig. 12).

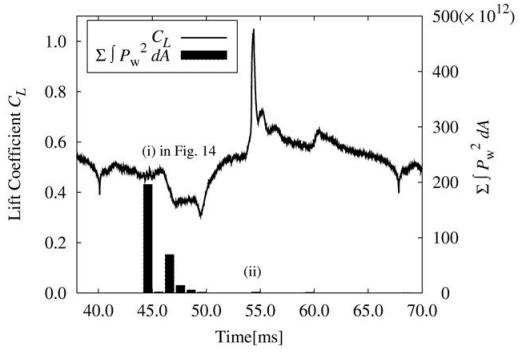

Figure 13: Variation of lift coefficient and $\Sigma \int P_w^2 dA$ every 1[ms] in one cycle of unsteady cavitating flow ($\sigma = 0.6$)

Finally, analysis of $\sigma = 1.1$ where small and large cloud cavities occur, is shown. Figures 15 and 16 show variation of C_L and $\Sigma \int P_w^2 dA$ every 1[ms] in one cycle of unsteady cavitating flow, and the time evolution of pressure distribution, isoline of void fraction 0.1, bubble positions and sizes at $\sigma = 1.1$, respectively. Large cloud cavity collapses at 65[ms] in the vicinity of the hydrofoil trailing edge as shown in Fig. 16 (i), (ii) and small cloud cavity collapses at 76[ms] more upstream than large cloud cavity, about $0.7 \leqq x/c \leqq 0.8$ as shown in Fig. 16 (iii), (iv). Impact energy occurs from the generation of each cloud cavity to the end of each cloud cavity collapse (Fig. 15). Although the behavior of large cloud cavity resembles that of the cloud at $\sigma = 1.0$ (Fig. 11), the generations of impact energy are some what different. At $\sigma = 1.0$ the bubbles in the vicinity of the sheet cavity termination are affected by the high pressure of cloud collapse and induce higher impact energy than impact energy induced by the bubbles in a cloud. On the other hand at $\sigma = 1.1$ it is found that impact energy induced by the bubbles in the vicinity of the sheet cavity termination is relatively small (63-65[ms] in Fig. 15). This is because the sheet cavity termination is far from the position of cloud collapse. E at 62-63[ms] is large because the large cloud exists on the

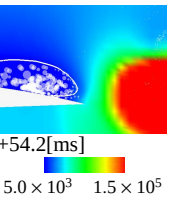

Figure 14: Time evolution of pressure distribution, isoline of void fraction 0.1, bubble positions and sizes ($\sigma = 0.6$)

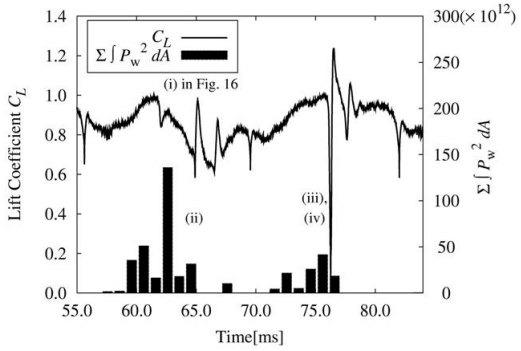

Figure 15: Variation of lift coefficient and $\Sigma \int P_w^2 dA$ every 1[ms] in one cycle of unsteady cavitating flow ($\sigma = 1.1$)

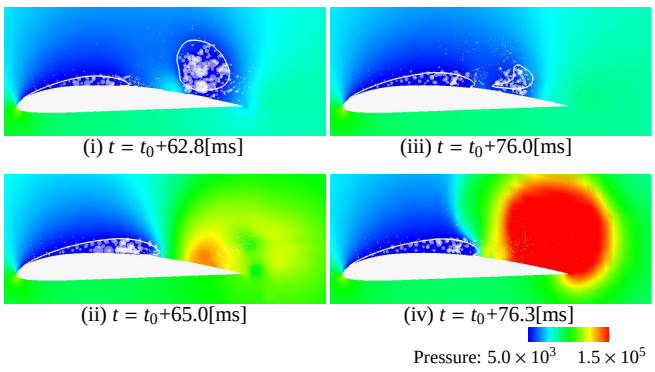

Figure 16: Time evolution of pressure distribution, isoline of void fraction 0.1, bubble positions and sizes ($\sigma = 1.1$)

hydrofoil from the beginning to the end of collapse, and the bubbles in the cloud induce the high impact energy. The bubbles in the cloud induce high impact pressure at the collapse of small cloud at 74-76[ms] as well as large cloud. But E is smaller than at the collapse of large cloud because the number of bubble in small cloud is smaller than in large cloud.

As stated above occurrence of high impact energy can be mainly divided into two cases as follows:
(i) Bubbles in a cloud induce high impact pressure during the cloud collapse. High impact energy only occurs if the cloud collapses near the hydrofoil.
(ii) Bubbles in the vicinity of sheet cavity termination induce high impact pressure owing to high pressure of cloud collapse. High impact energy only occurs if the length of sheet cavity is smaller than a chord length and the sheet cavity termination is close to the position of cloud collapse.
Higher impact pressure occurs when number of bubble in a cloud in case (i) and in the vicinity of the sheet cavity termination in case (ii) are large, in other words, when larger cloud cavity collapses in case (i) and thicker sheet cavity exists in case (ii). At $\sigma = 1.0$ the cloud cavity is the largest in case (i) and the sheet cavity is the thickest in case (ii). Therefore it is thought that the impact energy at $\sigma = 1.0$ becomes the largest in this study (Fig. 8).

CONCLUSION

Prediction method of cavitation erosion using one-way coupling method of analyses of cavitating flow field and bubble motion in the flow is proposed. In this prediction method, impact pressures acting on material surface are evaluated by pressure waves radiated by bubble collapse and rebound, and cavitation erosion is predicted by the impact energies. The cavitating flow around ClarkY 11.7 % hydrofoil at several cavitation number is picked up to examine our prediction method. The results are summarized as follows:

1. At $0.5 \leqq \sigma \leqq 1.2$ where transient cavitating flow occurs, when σ is large the sheet cavity is short, the cloud cavity collapses more upstream, and the flow field shows more complex behavior of interaction between cloud and sheet cavities.

2. The impact energy is small at $\sigma \geqq 1.3$ or $\sigma \leqq 0.4$ where the flow field is attached cavitating flow or pseudo supercavitating flow.

3. There is the obvious spatial peak value of impact energy and the position moves to downstream along with the decrease in σ at $1.0 \leqq \sigma \leqq 1.2$, and there is not the obvious peak value and weak erosion occurs on wide suction surface of the hydrofoil at $0.6 \leqq \sigma \leqq 0.8$.

4. High impact energy is mainly induced by bubbles in a cloud and in the vicinity of sheet cavity termination.

ACKNOWLEDGEMENT

The numerical simulations were performed by the super computer, Altix3700Bx2 in the Institute of Fluid Science, Tohoku University.

NOMENCLATURE

c: chord length
C: speed of sound
C_L: lift coefficient
D_a: density ratio of air in gas phase
e: total energy per unit volume
E: total energy of cavitation impacts
p: pressure
P_w: impact pressure
R: bubble radius
t: time
T: temperature
Y: mass fraction of gas
u_i: velocity vector
α: void fraction
ρ: density
σ: cavitation number

subscripts

0: initial
a: air
g: gas
in: main flow
l: liquid
m: gas-liquid mixture phase
v: vapor

REFERENCES

[1] Szkodo, M., 2005, "Mathematical Description and Evaluation of Cavitation Erosion Resistance of Materials", J. Materials Processing Tech., 164-165, 1631-1636.

[2] Franc, J. P., and Riondet, M., 2006, "Incubation Time and Cavitation Erosion Rate of Work-Hardening Materials", Proc. 6th Int. Symp. on Cavitation CAV2006, Wageningen, The Netherlands.

[3] Dular, M., Stoffel, B., and Sirok, B., 2006, "Development of a Cavitation Erosion Model", Wear, 261, 642-655.

[4] Fukaya, M., Tamura, Y., and Matsumoto, Y., 2006, "Prediction of Cavitation Intensity in Centrifugal Pump Based on Cavitating Flow Simulation Using Bubble Flow Model", Proc. 55th Nat. Cong. of Theoretical and Applied Mechanics, 111-112 (in Japanese).

[5] Hickling, R., and Plesset, M. S., 1964, "Collapse and Rebound of a Spherical Bubble in Water", Phys. Fluids, 7-1, 7-14.

[6] Fujikawa, S., and Akamatsu, T., 1978, "Experimental Investigation of Cavitation Bubble Collapse by a Water Shock Tube", Bulletin of the JSME, 21, 223-230.

[7] Naude, C. F., and Ellis, A. T., 1961, "On the Mechanism of Cavitation Damage by Nonhemispherical Cavities Collapsing in Contact With a Solid Boundary", ASME J. Basic Eng., 83, 648-656.

[8] Plesset M. S., and Chapman R. B., 1971, "Collapse of an Initially Spherical Vapour Cavity in the Neighbourhood of a Solid Boundary", J. Fluid Mech. , 47-2, 283-290.

[9] He, J.-G., and Hammitt, F. G., 1982, "Velocity Exponent and Cavitation Number for Venturi Cavitation Erosion of 1100-O Aluminum and 1018 Carbon Steel", Wear, 80, 43-58.

[10] Van der Meulen, J. H. J., and Nakashima, Y., 1983, ”A Study of the Relationship Between Type of Cavitation, Erosion and Luminescence”, Proc. 2nd Int. Conf. on Cavitation, 13-19.

[11] Okuda, K., and Ikohagi, T., 1996, ”Numerical Simulation of Collapsing Behavior of Bubble Cloud”, Transaction of the JSME Series B, 62(603), 3792-3797 (in Japanese).

[12] Iga, Y., Nohmi, M., Goto, A., Shin, B. R., and Ikohagi, T., 2003, ”Numerical Study of Sheet Cavitation Breakoff Phenomenon on a Cascade Hydrofoil”, ASME J. Fluids Eng., 125, 643-651.

[13] Shima, E., and Jounouchi, T., 1994, ”Role of Computational Fluid Dynamics in Aeronautical Engineering(No. 12) - Formulation and Verification of Uni-Particle Upwind Schemes for the Euler Equations -”, NAL-SP27, Proc. 12th NAL Symp. on Aircraft Computational Aerodynamics, 255-260.

[14] Anderson, W. K., Thomas, J. L., and van Leer, B., 1986, ”Comparison of Finite Volume Flux Vector Splittings for the Euler Equations”, AIAA J., 24-9, 1453-1460.

[15] Degani, D., and Schiff, L., 1986, ”Computation of Turbulent Supersonic Flows Around Pointed Bodies Having Crossflow Separation”, J. Computational Physics, 66, 176-196.

[16] Keller, J. B., and Kolodner, I. I., 1956, ”Damping of Underwater Explosion Bubble Oscillations”, J. Applied Physics, 27-10, 1152-1161.

[17] Yasui, K., 1996, ”Variation of Liquid Temperature at Bubble Wall near the Sonolumenescence Threshold”, J. Phys. Soc. Jpn., 65, 2830-2840.

[18] Theofanous, T. G., Biasi, L., Isbin, H. S., and Fauske, H. K., 1970, ”Nonequiblium Bubble Collapse: A Theoretical Study”, Chem. Engng. Progr. Symp. Ser., 66, 37-47.

[19] Numachi, F., Tsunoda, K, and Chida, I., 1949, ”Cavitation Tests on Six Profiles for Blade Elements”, The Rep. Institute of High Speed Mech., Tohoku Univ., 1-1, 1-16.

[20] Soyama, H., Kumano, H., and Saka, M., 2001, ”A New Parameter to Predict Cavitation Erosion”, Proc. 4th Int. Symp. Cavitation CAV2001, Pasadena, USA.

[21] Ito, Y., Oba, R., Soyama, H., Ogata, H., Okamura, T., Sudo, S., and Ikeda, R., 1988, ”A Study on Cavitation-Scale-Effects, Especially With Respect to Cavitation-Induced Pressure-Pulses”, Proc. Int. Symp. on Scale Modeling, Tokyo, Japan, 141-146.

[22] Magaino, A., Tamiya, S., Kato, H., and Maeda, M., 1979, ”Cavitation Erosion on a Two-Dimensional Hydrofoil (2nd Report)”, J. the Society of Naval Architects of Japan, 146, 101-111 (in Japanese).